Symmetry breaking and multiplicity of states in small aspect ratio Taylor–Couette flow

T. Mullin
Manchester Center for Nonlinear Dynamics, University of Manchester, Oxford Road, Manchester M13 9PL, United Kingdom

Y. Toya
Department of Mechanical Engineering, Nagano National College of Technology, Nagano, 381-8550, Japan

S. J. Tavener
Department of Mathematics, Colorado State University, Fort Collins, Colorado 80523

(Received 6 February 2002; accepted 25 April 2002; published 2 July 2002)

We report the results of an experimental and numerical study of the bifurcation structure of steady cellular states in small aspect ratio Taylor–Couette flows. In particular we focus on Z_2 symmetry-breaking bifurcations where asymmetric states which break the mid-plane symmetry arise. We find good quantitative agreement between numerical and experimental results for the bifurcation set. The surprising new observation we make is that the symmetry-breaking bifurcation sequences coalesce in a self-consistent way as the aspect ratio is reduced so that only symmetric steady flows exist for very short cylinders. The implications of this for the onset of disordered motion are discussed. © *2002 American Institute of Physics.* [DOI: 10.1063/1.1485997]

I. INTRODUCTION

Multiplicity in fluid flows is a feature of the Navier–Stokes equations which is of considerable scientific and practical importance. For example, either disordered or steady laminar flow can exist at the same Reynolds numbers (Re) for different realizations of an experiment or numerical simulation.[1] The state which is realized depends on the history of its evolution, i.e., the path which is taken through control parameter space. A familiar and readily demonstrated example of this is to be found in the flow between concentric cylinders where the inner rotates, which is commonly called the Taylor–Couette problem. Coles[2] provided clear evidence for multiplicity in the time-dependent regime where dynamically different states were realized with the same boundary conditions. These observations were later extended to include multiplicity in steady flows by Burkhalter and Koschmeider[3] and Benjamin and Mullin,[4] who uncovered a wide range of steady cellular states at modest Re. The situation with both cylinders rotating provides an even richer structure as shown by Andereck, Liu, and Swinney[5] and a review of all of this work may be found in Ref. 6.

Symmetry-breaking pitchfork bifurcations are particularly simple bifurcations which give rise to multiplicity of steady states. Pairs of solutions that break the mirror plane Z_2 symmetry arise at such bifurcations and they appear to be relatively common in fluid flows. Examples of these are in flow through a sudden expansion,[7,8] electrohydrodynamic convection in nematic liquid crystals,[9] and swirling flows.[10]

Taylor–Couette flow also provides a laboratory system where Z_2 symmetry-breaking pitchfork bifurcations occur and, importantly, detailed experimental datasets can be obtained, and these may be used to provide absolute comparisons with the results of numerical studies of the Navier–Stokes equations on physically relevant boundary conditions (see the review by Cliffe, Spence, and Tavener[11]). The symmetry breaking takes place on nontrivial symmetric cellular flows where one-half of the pattern grows at the expense of the other as Re is varied. As in any physical system, the effects of imperfections are present and one symmetry broken state grows continuously. The second disconnected state is thereby terminated by a fold or saddle node bifurcation. Unlike the onset of cells, the disconnection is small and is generally of the order of a few percent so that both asymmetric states can be readily produced in practice.

Symmetry-breaking bifurcations are known to be important in the organization of the dynamics found at higher Re as reviewed by Mullin.[12] The low-dimensional dynamics observed in neighboring ranges of Re are organized through the underlying steady solution structure via Silnikov dynamics as shown by Mullin and Price.[13] More recently, Abshagen, Pfister, and Mullin[14] have shown that gluing bifurcations resulting from Z_2 symmetry broken states are important over a much wider range of parameter space than had previously been appreciated. An explanation of the dynamics which can arise at gluing bifurcations is given by Glendinning, Abshagen, and Mullin.[15]

We will focus on symmetry breaking in steady flows in a particularly simple version of the Taylor–Couette problem where the gap between the two cylinders is comparable with the length of the flow domain. Thus the aspect ratio of the system is $\mathcal{O}(1)$ where we define the aspect ratio as $\Gamma = l/d$, where l is the length of the system and $d = r_o - r_i$ (where r_i and r_o are the radii of the inner and outer cylinders respectively) is the width of the gap between the cylinders. At small Re a pair of Ekman vortices dominate the flow field and this flow will be referred to as a steady two-cell flow. It

 © 2002 American Institute of Physics

Downloaded 18 May 2013 to 129.82.52.31. This article is copyrighted as indicated in the abstract. Reuse of AIP content is subject to the terms at: http://pof.aip.org/about/rights_and_permissions

was shown by Benjamin and Mullin[16] that this two-cell flow bifurcates into a pair of single-cell states when Re is increased through a Z_2 symmetry-breaking pitchfork bifurcation. The resulting asymmetric states break the mirror-plane symmetry of the stationary end boundary conditions and these flows were termed single-cell states since they were identified as such by Cliffe[17] in computations of the periodic model. These single-cell flows have been the subject of a great deal of subsequent numerical and experimental study, as reviewed by Pfister *et al.*,[18] Toya *et al.*,[19] and Furukawa *et al.*[20]

The outline of the article is as follows. We first describe the experimental and numerical bifurcation techniques used to study the flows. This is followed by a discussion of the bifurcation set for a particular radius ratio where we show good quantitative comparison between theory and experiment. The main conclusion we draw is that the flow is, rather surprisingly, unique and symmetric at very small aspect ratios. We then discuss the results of a numerical investigation of the effect of the radius ratio on this finding.

The apparent uniqueness of the flow implies that the robust routes to chaos via global homoclinic and gluing bifurcations found at larger aspect ratios will not be present in very short cylinders. Indeed, neither can simple period doubling occur for symmetric systems of this type as shown by Swift and Wiesenfeld.[21] Time dependence and disorder is observed in the flow at higher Re, but an understanding of its evolution remains an outstanding challenge.

II. EXPERIMENTAL APPARATUS AND NUMERICAL METHODS

A. Experimental apparatus

The experimental rig consisted of a pair of concentric cylinders which were mounted in a temperature-controlled environment. The outer cylinder was a precision bore quartz tube which had an inner diameter 74.6 ± 0.02 mm. The inner cylinder was made from stainless steel and machined to a diameter of 57.3 ± 0.02 mm so that the radius ratio, $\eta = r_i / r_o$, was 0.70. It was centered in sealed ball races which were located in two 10 mm thick aluminum end plates. The inner cylinder was driven round by a stepping motor via a gear box and belt drive system. The motor was controlled by an oscillator whose stability was better than 0.01% and the rotation speed of the cylinder was monitored and calibrated. The ends of the annular gap were defined by two stationary PTFE collars which bridged the annulus with 0.02 mm gaps at each wall. The upper collar was attached to a pair of rods which could be moved up and down using a micrometer screw gauge. The aspect ratio was measured using an external cathetometer and this was also used to observe the visualized flow structure.

The fluid was a water glycerol mixture whose viscosity was measured to be 5.63 cSt. The cylinders were surrounded by a water bath whose temperature was held at $27 \pm 0.02\,^{\circ}\mathrm{C}$ by fluid pumped through by a commercial temperature controller. The flow was visualized using Mearlmaid AA pearlessence and illumination was provided by a plane of light from a slide projector. The cellular structure was then clearly visible with well-defined thin dark interfaces between cells in the two-cell state. The position of the interface was measured using the cathetometer and was used as the measure to distinguish between flow states and detect departures from symmetry.

The control parameters for the system are the aspect ratio and the Reynolds number. We define the latter as $\mathrm{Re} = (\Omega r_i d)/\nu$, where ν is the kinematic viscosity of the fluid. The Reynolds number and aspect ratio are, in principle, continuously variable parameters, but in practice, they were changed in very small discrete steps with long settling times allowed between changes. The waiting times were established empirically using repeatability of critical points as the criterion, and ranged from minutes away from critical points to hours near bifurcations.

In the appropriate range of aspect ratios, increase in Re led to the continuous appearance of an asymmetric state over a small range of Re. In this, one cell grew at the expense of the other and the direction of the growth was always the same because the bifurcation was disconnected by the presence of imperfections. It should be noted that physical imperfections will be present in any experimental system and the asymmetric states do not arise as a result of them. The state with the opposite asymmetry could be achieved by sudden starts of the system or other discontinuous changes in parameters, and then estimates of the symmetry-breaking bifurcation points were obtained by measuring the saddle-node points where the asymmetric states collapsed to the symmetric ones by reduction in Re. Variations on this theme were used to obtain estimates for all the other bifurcation points. The essential feature is that the experimental points correspond to catastrophic changes in the flow structure with change in Re and these were used to compare with the numerical results where perfect symmetry was assumed.

B. The finite-element technique

Numerical solutions of the steady axisymmetric Navier–Stokes equations with no-slip boundary conditions and the locations of singular points were calculated using the finite-element package ENTWIFE.[22] The computational domain was a cross section of the annular gap between the two cylinders. The domain was discretized using a 24×40 finite-element mesh which, with the exception of the corners, was uniform over the domain. The finite-elements used were nine-noded quadrilateral elements with biquadratic velocity and discontinuous linear pressure interpolation. Suitable corner refinements were employed to take into account the rapid change in velocity between the moving and stationary walls in two of the corners. Doubling the number of elements in each direction produced a less than 0.01% change in the computed locations of the bifurcation points and so we are confident that the solutions are numerically resolved on the 24×40 grid. Cliffe, Spence, and Tavener[11] present a comprehensive discussion of numerical bifurcation techniques for the Navier–Stokes equations. An earlier discussion by Cliffe

Downloaded 18 May 2013 to 129.82.52.31. This article is copyrighted as indicated in the abstract. Reuse of AIP content is subject to the terms at: http://pof.aip.org/about/rights_and_permissions

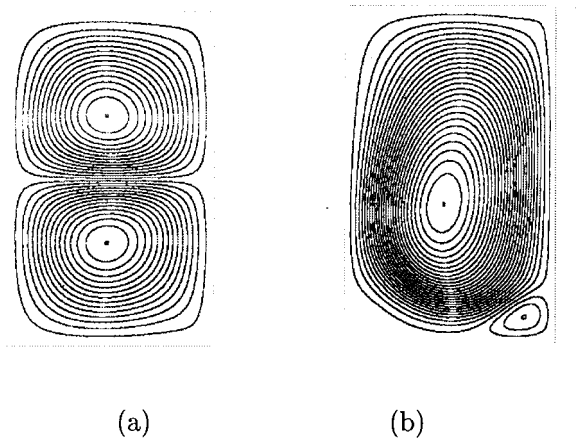

FIG. 1. Streamline plots for two-cell and single-cell states using 30 equally spaced values of the streamfunction. The radius ratio is 0.7. The right-hand side of each figure corresponds to the rotating inner cylinder. (a) $\Gamma=1.6$, Re=200. The direction of rotation of the upper vortex is clockwise. (b) $\Gamma=1.6$, Re=500. The direction of rotation of the main vortex is clockwise.

and Spence[23] concentrates on numerical computation of symmetry-breaking phenomena in the Taylor–Couette system.

III. RESULTS

We now discuss the application of the experimental and numerical techniques described above to the study of pitchfork bifurcations in a small aspect ratio Taylor–Couette system. Our results are concerned with two- and single-cell flows and the exchange of stability between them as the aspect ratio is varied. We show two ''typical'' streamline plots of the states involved in the interaction in Fig. 1. It should be noted that the single-cell plot contains an additional secondary vortex in the bottom right-hand corner of the flow domain. In fact, they exist in all four corners, but the value of the streamfunction associated with these recirculations is so small in magnitude that they do not appear in the plots. They are a necessary consequence of the no-slip boundary condition and are essential to all states on finite domains. Despite the presence of these extra vortices we refer to these states as single-cell flows since it has been shown by Cliffe[17] that they originate at pitchfork bifurcations to one cell flows in the periodic problem.

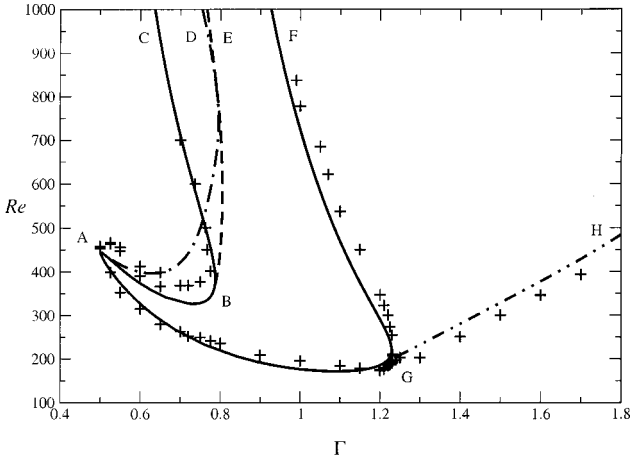

FIG. 2. Comparison between experimental and numerical results for transitions of one- and two-cell steady flows. The solid line is a path of symmetry-breaking bifurcation points. The chained and dashed lines are paths of limit points. Note that the two curves AD and BE do not meet or cross but just appear to do so on the scale used here.

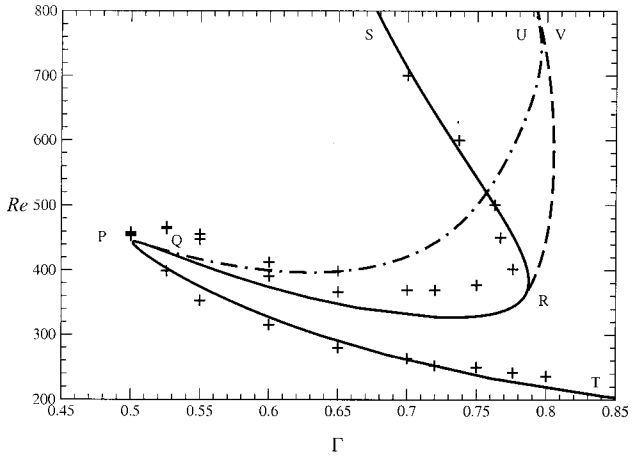

FIG. 3. Expanded view of the left-hand side of the bifurcation set.

Much of this bifurcation structure has been calculated and observed previously by Cliffe,[17] Pfister *et al.*,[18] and Benjamin and Mullin[16] for the radius ratio $\eta=0.5$. However, the present experimental results are for a narrower gap ($\eta=0.7$), and during this investigation important new features came to light which were missed in the earlier studies. Part of the reason they were not identified earlier is that they exist primarily at large Reynolds numbers for wide gaps. However, they are essential features of the solution structure over the entire range of radius ratios. We have therefore investigated their properties using a numerical bifurcation study of the effects of radius ratio on the bifurcation set.

A. The numerical and experimental bifurcation set for $\eta=0.7$

We show in Fig. 2 the full steady bifurcation set in the (Γ, Re) plane for the one-cell, two-cell interaction for $\eta=0.7$. The lines have been calculated using the methods discussed above and the crosses are experimental points. It can be seen that there is very good overall agreement between the numerical and experimental results. Before discussing these results in depth we will first focus on the novel bifurcation structure found in the present investigation at very small aspect ratios. The most important of the new features are highlighted in a blow-up of the left-hand side of the full bifurcation set, shown in Fig. 3.

We have relabelled Fig. 3 in order to avoid confusion with the labelling of the full bifurcation set, and the point marked P in Fig. 3 is equivalent to A in Fig. 2. The line marked TPQRS is the path of symmetry-breaking pitchfork bifurcations on the two-cell state. This bifurcation is supercritical between T and P, P and Q, and R and S and is sub-

Downloaded 18 May 2013 to 129.82.52.31. This article is copyrighted as indicated in the abstract. Reuse of AIP content is subject to the terms at: http://pof.aip.org/about/rights_and_permissions

critical between Q and R. It is at these symmetry-breaking bifurcations that single-cell flows are created or destroyed by increase of the Reynolds number. The loci labeled QU and RV are paths of limit points (folds) along branches of single-cell states. Note that the crossing of RS and QU is merely a projection artifact and does not represent a further bifurcation. The path of limit points QU meets the line of symmetry-breaking bifurcations at Q which is therefore a point of codimension-2. Similarly, RV meets TPQRS at R which is also a codimension-2 point.

We show in Fig. 4 a sequence of qualitatively different bifurcation diagrams which have been calculated at seven fixed values of the aspect ratio. The ordinate in each is the axial velocity at the center of a radial slice, i.e., at $(r,z)=(0.5,0)$. Stable solutions are indicated with "s," unstable solutions with "u," where instability is with respect to stationary disturbances which break the Z_2 symmetry. We will use these to aid our discussion of the bifurcation sets. In the aspect ratio range to the left of P a normal two-cell flow is the only stable steady axisymmetric state for all practical Reynolds numbers, i.e., symmetry broken steady single-cell states do not exist in the wide range of Re studied here. An anomalous two-cell flow, where the directions of the streamlines are reversed, must also exist, but it does so at a Reynolds number which is at least an order of magnitude greater than is of interest here.

The schematic bifurcation diagram in Fig. 4(a) is relevant to the aspect ratio range to the immediate right of the point labeled P in Fig. 3. PT is a path of symmetry-breaking bifurcations at which pairs of single-cell flows arise with increase of Re. The bifurcation is necessarily imperfect in the experiment and the marked experimental points correspond to the saddle node of the disconnected branch. This was reached, in the experiment, by sudden starts of the inner cylinder and estimates of the saddle node were then obtained by slow reduction in Re until a catastrophic collapse of the state was observed. As the aspect ratio was reduced, such that the point P was approached, the observations became more difficult to perform since the physical height of the gap was $\sim$4 mm. Despite the difficulties, repeatable measurements were obtained when suitable care was taken.

For aspect ratios corresponding to the range P to Q it was found that, after the initial formation of an asymmetric flow, further increase in Re led to the smooth reformation of the symmetric two-cell state. This is consistent with the bifurcation diagram Fig. 4(a), where forward and reverse supercritical symmetry-breaking bifurcations are shown. Again, imperfections are important in the experimental observations, and hence there is an offset between the experiments and numerics. However, the principal result that P is a coalescence point is clear. Hence, we conclude that the only steady axisymmetric flows at smaller aspect ratios comprise two cells and we speculate that they are unique.

As Γ is increased to values greater than Q in Fig. 3, the second pitchfork bifurcation becomes subcritical as shown in Fig. 4(b). The symmetry-breaking bifurcation has quartic contact at Q and is subcritical for larger values of Γ. There is now hysteresis in the reemergence of the two-cell states at fixed values of Γ when Re is increased and decreased. QU is the path of limit points for the pairs of one-cell states and there is confirming evidence for this feature in the experimental data. However, the effects of imperfections are now greater and the experiment was further complicated by the onset of oscillations. The oscillations had the form of a three-dimensional wave and were found for $\Gamma>0.65$. The time dependence and associated Hopf bifurcations are the subject of ongoing research. The agreement between calculation and experiment is satisfactory when one takes into account that the hysteresis is present over a physical length scale of <1 mm.

As Γ was increased above $\Gamma\approx0.65$, the symmetric flow which arose after the second symmetry-breaking bifurcation remained steady while the single-cell states were both time-dependent as discussed above. The two-cell flow was readily established above PR either by sudden starts or by suitable changes in both Γ and Re. Estimates of PR were then found by reducing Re until a catastrophic collapse to a time-dependent one-cell state was found. On the other hand, the almost vertical section RS was detected more readily by fixing Re and incrementing Γ in very small steps under micrometer control. As in all other cases, sufficient time was allowed between parameter changes for equilibrium to be established after each small step. RS corresponds to the path of a third symmetry-breaking bifurcation which is the third pitchfork at the right-hand side of Fig. 4(c). A pair of stable one-cell states arise at this bifurcation and they were detected in the experiment by observing where departures from symmetry occurred as Γ was increased. Excellent agreement between experimental and numerical results was obtained.

Several features of the bifurcation diagram presented in Fig. 4(c) deserve further comment. The apparent intersections between the branches which arise at the first two pitchfork bifurcations are merely an artifact of projection and thus do not signify bifurcations. The clear pair of kinks in the branches which arises at the third pitchfork is significant and it corresponds to a pair of folds in the solution surface. The upper folds correspond to the path of limit points RV in Fig. 3 (BE, Fig. 2) and the lower ones correspond to QU in Fig. 3 (AD, Fig. 2). Note that they are outside of the parameter range shown in Fig. 3 but are included in Fig. 2. It may at first sight seem odd that these two distinct paths of bifurcation points in Fig. 3 are closely linked in this particular bifurcation diagram, but, as will be discussed later, this allows the branches arising at the second and third pitchforks to join at larger aspect ratio.

The coalescence of the second and third pitchforks takes place between the bifurcation diagrams shown in Figs. 4(d) and 4(e), i.e., in the aspect ratio range 0.787 to 0.79. Before coalescence can occur, the two pitchforks must have opposite curvature locally and thus the second pitchfork becomes supercritical with an associated, but small, amount of hysteresis as shown in Fig. 4(d). Coalescence takes place as Γ is increased, resulting in the bifurcation diagram shown in Fig. 4(e). The limit points formed at the quartic point correspond to the lower section of the locus labeled RV in Fig. 3. Further increase in Γ leads to the rapid joining of the outer folded surfaces of Fig. 4(e) at a transcritical bifurcation point at $(\Gamma,\mathrm{Re})\approx(0.796,740)$, which then disconnects as Γ is in-

Downloaded 18 May 2013 to 129.82.52.31. This article is copyrighted as indicated in the abstract. Reuse of AIP content is subject to the terms at: http://pof.aip.org/about/rights_and_permissions

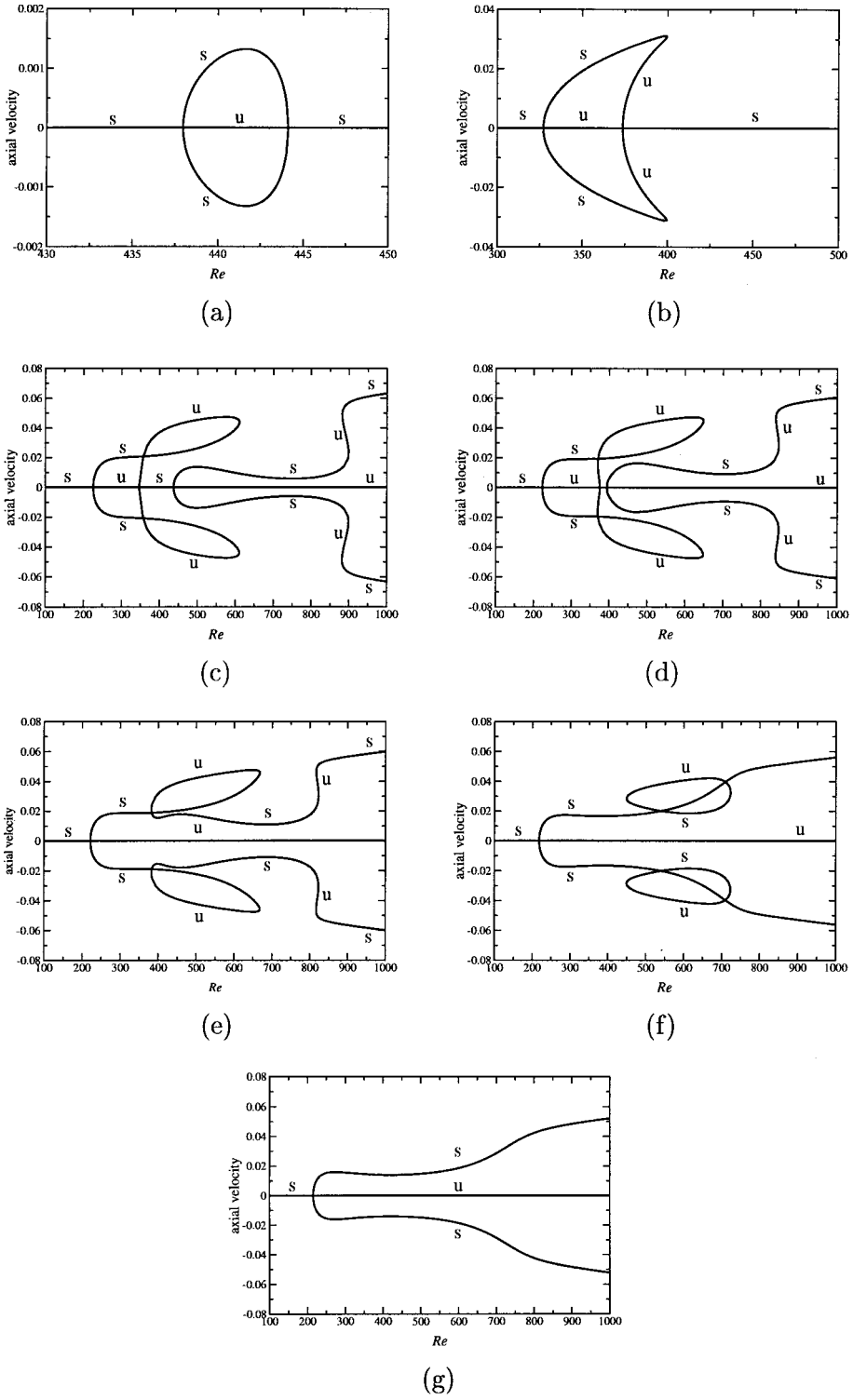

FIG. 4. Computed bifurcation diagrams for $\eta=0.7$ and (a) $\Gamma=0.5025$, (b) $\Gamma=0.6$, (c) $\Gamma=0.78$, (d) $\Gamma=0.787$, (e) $\Gamma=0.79$, (f) $\Gamma=0.8$, and (g) $\Gamma=0.81$. The ordinate is the axial velocity at $(r,z)=(\frac{1}{2},0)$. Stable solutions are indicated with "s," unstable solutions with "u" where instability is with respect to stationary disturbances which break the Z_2 symmetry.

creased such that a pair of isolated loops of solutions is left, as is shown in Fig. 4(f). The upper and lower limit points of these closed loops of solutions lie on the path labeled RV in Fig. 3. Yet further increase in Γ leads to a rapid shrinking of these isolated loops to isola formation points at $(\Gamma,\mathrm{Re})\approx(0.805,580)$, where RV in Fig. 3 is perpendicular to the aspect ratio axis. For slightly larger values of Γ a pair of unfolded branches of single-cell states remains as shown in Fig. 4(g).

In Figs. 4(c)–4(f) there is a range of Re over which two forms of the single-cell state are stable. Examples of these flows are shown in the streamline plots in Fig. 5. Although

Downloaded 18 May 2013 to 129.82.52.31. This article is copyrighted as indicated in the abstract. Reuse of AIP content is subject to the terms at: http://pof.aip.org/about/rights_and_permissions

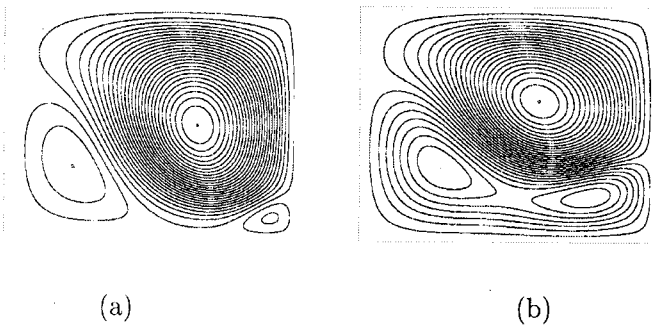

FIG. 5. Streamline plots for single-cell states calculated at $\Gamma=0.78$ and $\mathrm{Re}=600$ using 30 equally spaced values of the streamfunction. The rotating wall is on the right-hand side in both figures and the direction of rotation of the largest vortex is anticlockwise in each case. (a) Flow originating from the first pitchfork. (b) Flow arising at the third pitchfork.

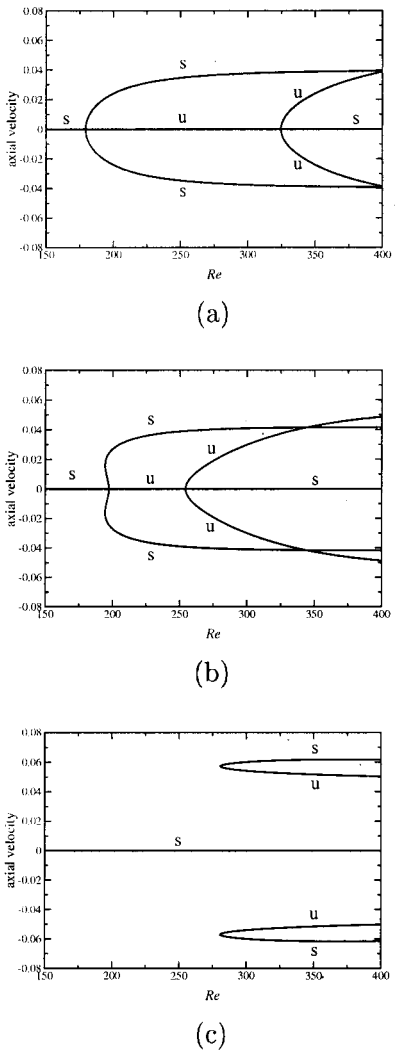

FIG. 6. Computed bifurcation diagrams for $\eta=0.7$ and (a) $\Gamma=1.18$, (b) $\Gamma=1.22$, and (c) $\Gamma=1.4$. The ordinate axis measures the axial velocity at $(r,z)=(0.4,0)$.

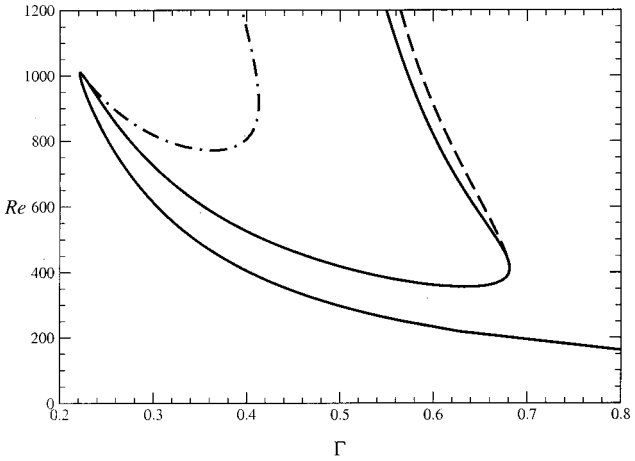

FIG. 7. Singular points at $\eta=0.5$. The solid line is a path of symmetry-breaking bifurcation points. The chained and dashed lines are paths of limit points.

we were unable to obtain definitive observations of the one shown in Fig. 5(b), such flows have been observed previously at other radius ratios by Nakamura and Toya.[24]

Returning to the discussion of the experimental results shown on the full bifurcation set in Fig. 2, we see that we have thus far described the structure associated with GABC (symmetry breaking) AD, and BE (saddle nodes). It is interesting to note that much of the above sequence of bifurcations in the parameter range around B in Fig. 2 is qualitatively the same as that proposed by Benjamin and Mullin[16] for the disconnection of one-cell flows found at larger aspect ratios. However, at these smaller aspect ratios the stabilities of the solutions involved in the interaction are reversed. The remainder of the bifurcation set shown in Fig. 2 for the aspect ratio range $\Gamma>1$ is completely in accord with previous studies. The two-cell state is restabilized by a second symmetry-breaking bifurcation as indicated in Fig. 6(a) and the path of this bifurcation is given by the numerical and experimental results labeled FG in Fig. 2. A coalescence takes place between the two symmetry-breaking bifurcations at G and there is a small but definite amount of hysteresis as depicted in Fig. 6(b). The merging of the two symmetry-breaking bifurcations leads to the disconnection of the single-cell states for greater values of Γ as shown in Fig. 6(c). Hence GH is a path of limit points and again good agreement is found between experimental and numerical results as can be seen in Fig. 2.

B. The effect of radius ratio

We first investigated the case of $\eta=0.5$ since this value was used in most previous studies and yet the existence of a coalescence point corresponding to A in Fig. 2 (P, Fig. 3) and the associated bifurcation structure has not been reported. The numerical results are shown in Fig. 7 where we focus on the range of Γ from 0.2 to 0.8 to highlight these new features. It can be seen that a coalescence of the pitchforks which give rise to single-cell states does occur at $(\Gamma,\mathrm{Re})\approx(0.21,1000)$ and the associated paths of limit points are also present as for $\eta=0.7$ and shown in Fig. 3. There are,

Downloaded 18 May 2013 to 129.82.52.31. This article is copyrighted as indicated in the abstract. Reuse of AIP content is subject to the terms at: http://pof.aip.org/about/rights_and_permissions

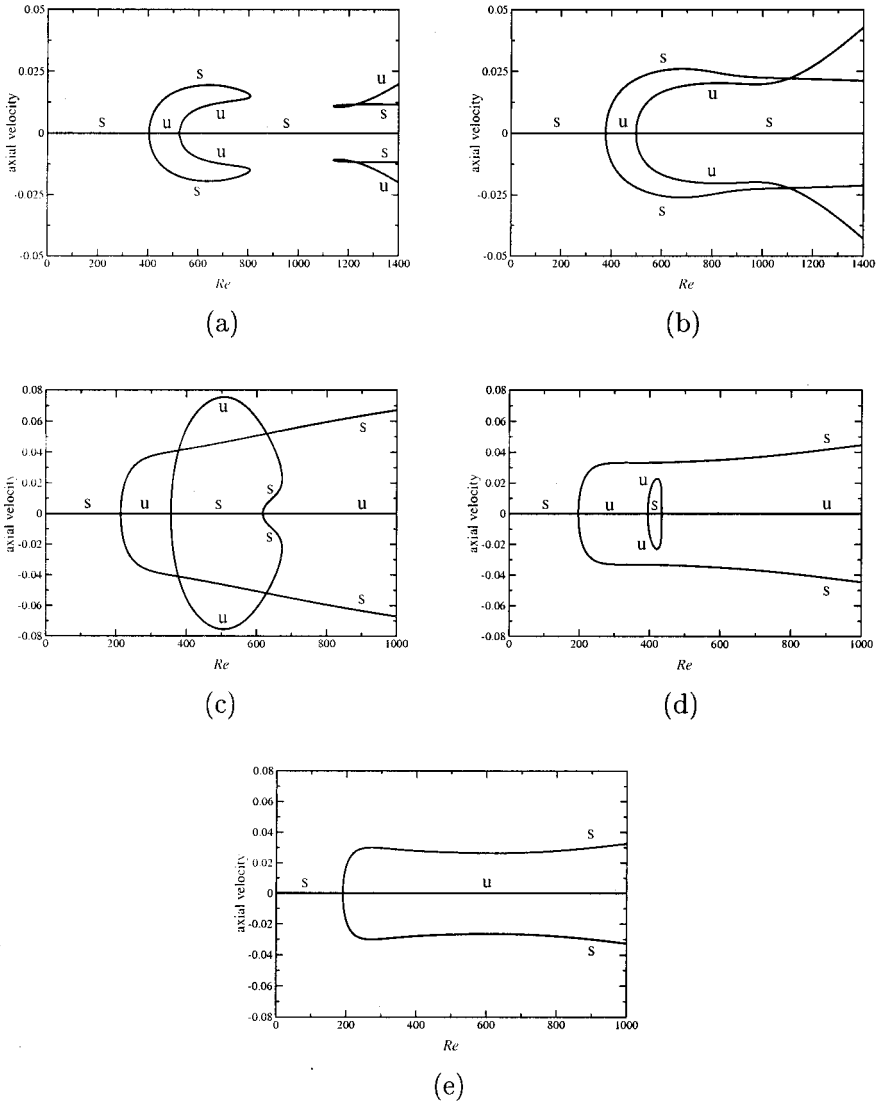

FIG. 8. Bifurcation diagrams at $\eta=0.5$ and (a) $\Gamma=0.4$, (b) $\Gamma=0.42$, (c) $\Gamma=0.64$, (d) $\Gamma=0.68$, and (e) $\Gamma=0.7$. The ordinate axis measures the axial velocity at $(r,z)=(0.4,0)$.

however, important detailed changes in the sequence of singularities which simplify the bifurcation set. The path of limit points which emerges near the coalescence point does not now cross the path of pitchforks as it does in Fig. 3 and the second path of limit points denoted by the dashed line emerges above the right-hand coalescence point of the second and third pitchforks.

A sequence of qualitatively distinct bifurcation diagrams

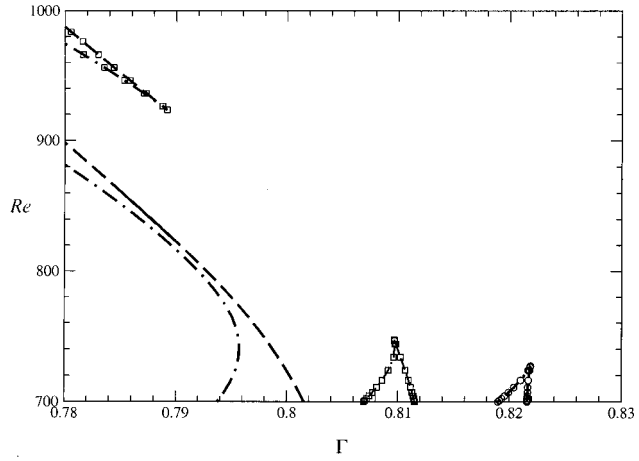

FIG. 9. Limit points at $\eta=0.7$ $(--)$, 0.71 (□), 0.72 (○). The paths of limit points merge and reseparate in the opposite manner between $\eta=0.7$ and $\eta=0.71$.

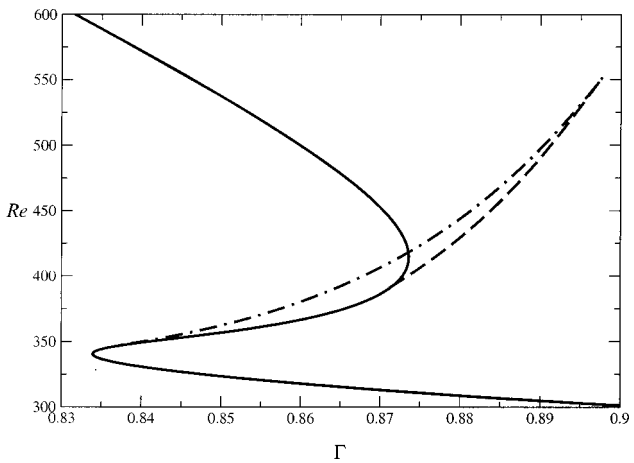

FIG. 10. Singular points at $\eta=0.85$. The solid line is a path of symmetry-breaking bifurcation points. The chained and dashed lines are paths of limit points.

Downloaded 18 May 2013 to 129.82.52.31. This article is copyrighted as indicated in the abstract. Reuse of AIP content is subject to the terms at: http://pof.aip.org/about/rights_and_permissions

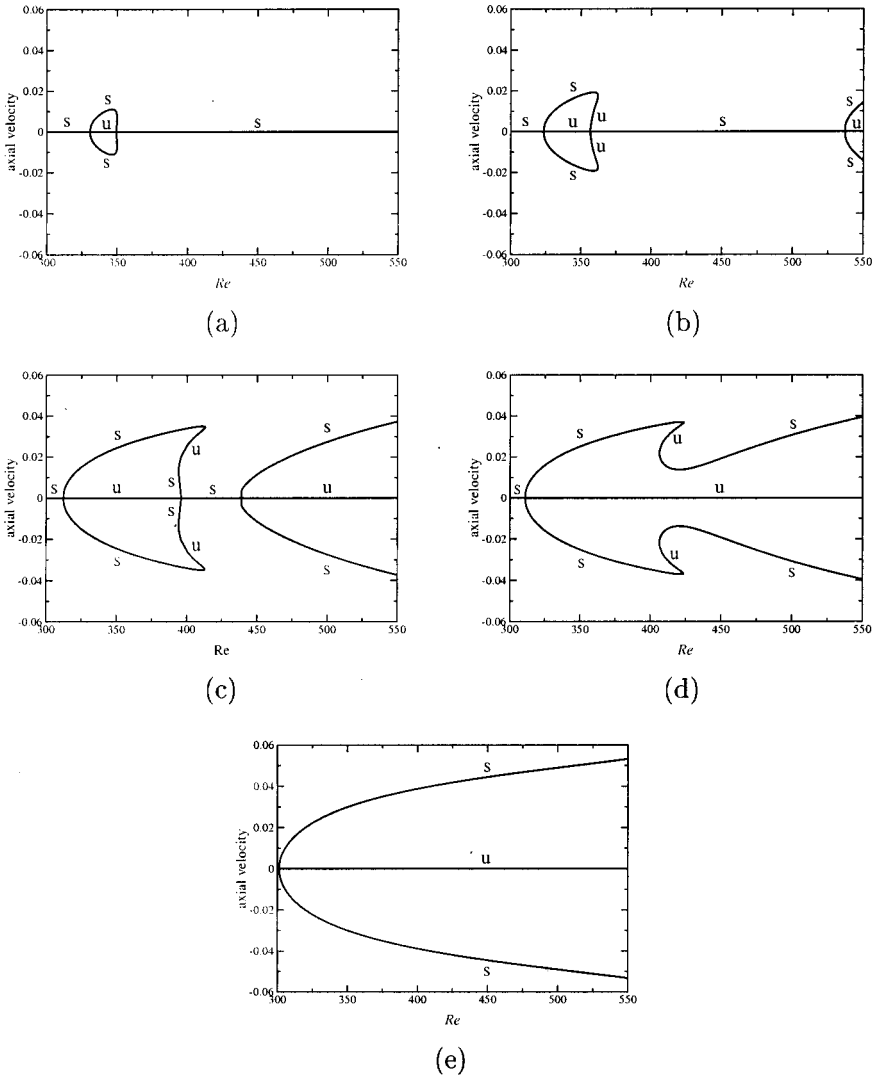

FIG. 11. Bifurcation diagrams for $\eta = 0.85$ and (a) $\Gamma = 0.84$, (b) $\Gamma = 0.85$, (c) $\Gamma = 0.872$, (d) $\Gamma = 0.875$, and (e) $\Gamma = 0.9$. The ordinate axis measures the axial velocity at $(r,z) = (\frac{1}{2},0)$.

which cover the aspect ratio range of Fig. 7 are given in Fig. 8. A diagram similar to Fig. 4(a) for aspect ratios slightly greater than that at the left-hand coalescence point has been omitted. As in Fig. 4(b), for aspect ratios exceeding that at the left-hand quartic bifurcation point, the first two pitchforks in the sequence are connected as shown in Fig. 8(a). On the right-hand side of this figure a pair of disconnected single-cell solutions are shown and these come in towards the single-cell solutions arising at the connected pitchforks with increasing Γ, and interact at a transcritical bifurcation. This transcritical bifurcation disconnects in the opposite sense, leaving a smoothly developing pair of solutions from the first pitchfork as shown in Fig. 8(b). Note that this transcritical bifurcation is not shown in Fig. 8(b). The crossing shown there is an artifact of the projection. The branches from the second pitchfork connect to those from the third pitchfork which comes in from large Re as Γ is increased, producing the bifurcation diagram at $\Gamma = 0.64$ shown in Fig. 8(c). Yet further increase in Γ leads to the collapse of the connected loop as shown in Figs. 8(d) and 8(e).

As the radius ratio η is increased above 0.7, the bifurcation set also becomes less complicated as some of the limit point structure disappears. This may be seen in Fig. 9 where details of the two paths of limit points AD and BE from Fig. 2 are now given at radius ratios of 0.7, 0.71, and 0.72. The two paths of limit points merge between radius ratios of 0.7 and 0.71 and then separate in the opposite sense. At a radius

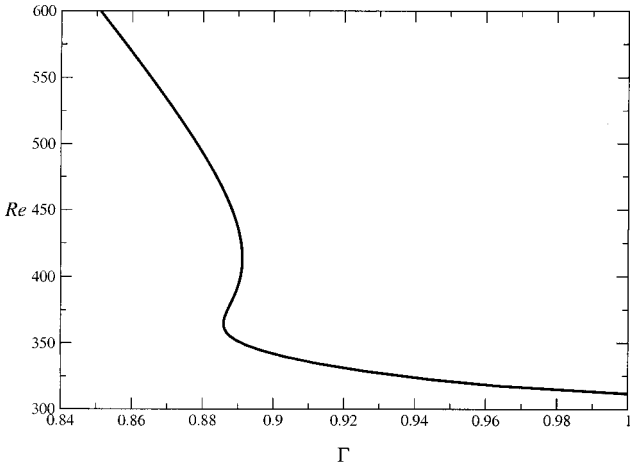

FIG. 12. Singular points at $\eta = 0.87$. The solid line is a path of symmetry-breaking bifurcation points.

Downloaded 18 May 2013 to 129.82.52.31. This article is copyrighted as indicated in the abstract. Reuse of AIP content is subject to the terms at: http://pof.aip.org/about/rights_and_permissions

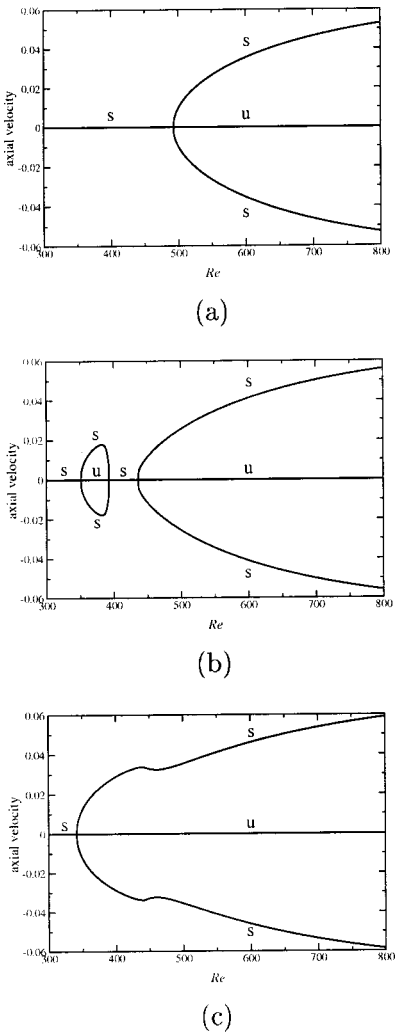

FIG. 13. Bifurcation diagrams for $\eta=0.87$ and (a) $\Gamma=0.88$, (b) $\Gamma=0.89$, and (c) $\Gamma=0.9$. The ordinate axis measures the axial velocity at $(r,z)=(\frac{1}{2},0)$.

ratio of 0.72, the upper paths of limit points exist only for Reynolds numbers exceeding 1000.

As the radius ratio increases beyond 0.72, the closed path of limit points at lower Reynolds number shrinks and the coalescence points A and B of Fig. 2 approach each other. The situation at a radius ratio of 0.85 is shown in Fig. 10. Computed bifurcation diagrams at a radius ratio of 0.85 and aspect ratios 0.84, 0.85, 0.872, 0.875, and 0.9 are shown in Fig. 11. It can be seen that near the bifurcation points the basic sequence found at other radius ratios remains the same, but the situation is much simplified at larger Reynolds number.

With further increase of the radius ratio beyond 0.85, the quartic bifurcation points merge, collapsing the closed path of limit points. The remaining locus of symmetry-breaking bifurcation points at a radius ratio of 0.87 is shown in Fig. 12. The considerably simplified sequence of bifurcation diagrams is shown in Fig. 13.

The two coalescence points A and B (Fig. 2) merge as the radius ratio is further increased and the unfolded path of symmetry-breaking bifurcation points at radius ratio 0.9 is shown in Fig. 14.

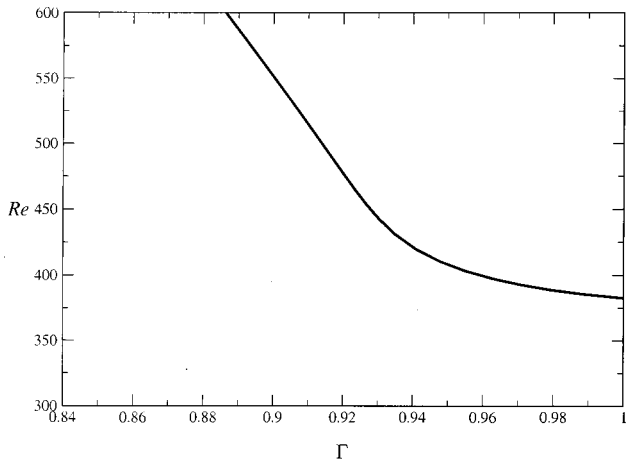

FIG. 14. Singular points at $\eta=0.9$. The solid line is a path of symmetry-breaking bifurcation points.

IV. CONCLUSION

The bifurcation sequences described earlier in this work show that as the aspect ratio is reduced so multiplicity in the solution set disappears systematically. Some of the bifurcation structure observed here is consistent with that observed previously for other values of the radius ratio. However, important new features have been uncovered which suggest that the flow may be symmetric and unique at small values of the aspect ratio. Indeed, preliminary numerical studies have shown that the parameter range over which this occurs expands greatly as the radius ratio increases.

This preference for symmetric flows in small-scale systems leads to interesting questions on the onset of disordered motion. Libchaber *et al.*'s[25] celebrated work on Rayleigh–Benard convection in domains with aspect ratios of $\mathcal{O}(1)$ suggests that period doubling will be prevalent in small-scale systems. Indeed it has also been shown to be the case for small aspect ratio Taylor–Couette flow.[26] However, it is known that symmetric systems, such as the two-cell flow, cannot undergo period-doubling sequences to chaos without first undergoing symmetry breaking.[21] Further, symmetry broken states contribute to other low-dimensional dynamics such as homoclinic and gluing bifurcations as discussed above and these no longer exist at very small aspect ratios. Preliminary observations of disordered motion have been made in our experiment at large Reynolds numbers, but we are, as yet, unable to account for the possible mechanisms which give rise to it. This is the subject of ongoing research.

[1] T. Mullin, "Disordered fluid motion in a small closed system," Physica D **62**, 192 (1993).
[2] D. Coles, "Transition in circular Couette flow," J. Fluid Mech. **21**, 385 (1965).
[3] J. E. Burkhalter and E. L. Koshmeider, "Steady supercritical Taylor vortex flow," J. Fluid Mech. **58**, 547 (1973).
[4] T. B. Benjamin and T. Mullin, "Notes on the multiplicity of flows in the Taylor experiment," J. Fluid Mech. **121**, 219 (1982).
[5] C. D. Andereck, S. S. Liu, and H. L. Swinney, "Flow regimes in a circular

Downloaded 18 May 2013 to 129.82.52.31. This article is copyrighted as indicated in the abstract. Reuse of AIP content is subject to the terms at: http://pof.aip.org/about/rights_and_permissions

Couette system with independently rotating cylinders,'' J. Fluid Mech. **164**, 155 (1986).
[6]R. Tagg, ''The Couette–Taylor problem,'' Nonlinear Sci. Today **4**, 1 (1994).
[7]R. M. Fearn, T. Mullin, and K. A. Cliffe, ''Nonlinear flow phenomena in a symmetric sudden-expansion,'' J. Fluid Mech. **211**, 595 (1990).
[8]J. Mizushima and Y. Shiotani, ''Bifurcation of flow in a channel with a sudden expansion,'' J. Fluid Mech. **420**, 131 (2000).
[9]T. Peacock and T. Mullin, ''Homoclinic bifurcations in a liquid crystal flow,'' J. Fluid Mech. **432**, 369 (2001).
[10]V. Shtern and F. Hussain, ''Instabilities of conical flows causing steady bifurcations,'' J. Fluid Mech. **366**, 33 (1998).
[11]K. A. Cliffe, A. Spence, and S. J. Tavener, ''The numerical analysis of bifurcation problems with application to fluid mechanics,'' Acta Numerica **39**, 39 (2000).
[12]T. Mullin, *The Nature of Chaos* (Clarendon, Oxford, 1993).
[13]T. Mullin and T. J. Price, ''An experimental observation of chaos arising from the interaction of steady and time-dependent flows,'' Nature (London) **340**, 294 (1989).
[14]J. Abshagen, G. Pfister, and T. Mullin, ''A gluing bifurcation in a dynamically complicated extended flow,'' Phys. Rev. Lett. **87**, 224501 (2001).
[15]P. Glendinning, J. Abshagen, and T. Mullin, ''Imperfect homoclinic bifurcations,'' Phys. Rev. E **64**, 036208 (2001).
[16]T. B. Benjamin and T. Mullin, ''Anomalous modes in the Taylor experiment,'' Proc. R. Soc. London, Ser. A **377**, 221 (1981).
[17]K. A. Cliffe, ''Numerical calculations of two-cell and single-cell Taylor flows,'' J. Fluid Mech. **135**, 219 (1983).
[18]G. Pfister, H. Schmidt, K. A. Cliffe, and T. Mullin, ''Bifurcation phenomena in Taylor-Couette flow in a very short annulus,'' J. Fluid Mech. **191**, 1 (1988).
[19]Y. Toya, L. Nakamura, S. Yamashita, and Y. Ueki, ''An experiment on a Taylor vortex flow in a gap with small aspect ratio,'' Acta Mech. **102**, 137 (1994).
[20]H. Furkawa, T. Watanabe, Y. Toya, and I. Nakamura, ''Flow pattern exchange in the Taylor–Couette system with a very small aspect ratio,'' Phys. Rev. E **65**, 036306 (2002).
[21]J. W. Swift and K. Wiesenfeld, ''Suppression of period-doubling in symmetric systems,'' Phys. Rev. Lett. **52**, 705 (1984).
[22]K. A. Cliffe, ENTWIFE Release 6.3 Reference Manual: ENTWIFE, INITIAL DATA and SOLVER DATA Commands; AEAT-0823 (1996).
[23]K. A. Cliffe and A. Spence, ''The calculation of high order singularities in the Taylor problem,'' in *Numerical Methods for Bifurcation Problems*, edited by T. Kupper, H. D. Mittelmann, and H. Weber (Birkauser, Basel, 1984), Vol. 70, p. 129.
[24]L. Nakamura and Y. Toya, ''Existence of extra vortex and twin vortex of anomalous mode in Taylor vortex flow with a small aspect ratio,'' Acta Mech. **117**, 33 (1996).
[25]A. Libchaber, C. Laroche, and S. Fauve, ''Period doubling cascade in mercury, a quantitative measurement,'' J. Phys. (France) Lett. **43**, L211 (1982).
[26]G. Pfister, A. Schulz, and B. Lensch, ''Bifurcations and a route to chaos of a one-vortex-state in Taylor–Couette flow,'' Eur. J. Mech. B/Fluids **10**, 247 (1991).

Downloaded 18 May 2013 to 129.82.52.31. This article is copyrighted as indicated in the abstract. Reuse of AIP content is subject to the terms at: http://pof.aip.org/about/rights_and_permissions